ACS APPLIED MATERIALS & INTERFACES

Research Article

www.acsami.org

Flexible Organic Light-Emitting Diodes with Enhanced Light Out-Coupling Efficiency Fabricated on a Double-Sided Nanotextured Substrate

Yu Luo,[†] Chunhui Wang,[†] Li Wang,*[,†] Yucheng Ding,*[,†] Long Li,[†] Bin Wei,[‡] and Jianhua Zhang[‡]

[†]State Key Laboratory for Manufacturing Systems Engineering, Xi'an Jiaotong University, Xi'an 710049, China

[‡]Key Laboratory of Advanced Display and System Applications, Shanghai University, Shanghai 200072, China

ABSTRACT: High-efficiency organic light-emitting diodes (OLEDs) have generated tremendous research interest. One of the exciting possibilities of OLEDs is the use of flexible plastic substrates, which unfortunately have a mismatching refractive index compared with the conventional ITO anode and the air. To unlock the light loss on flexible plastic, we report a high-efficiency flexible OLED directly fabricated on a double-sided nanotextured polycarbonate substrate by thermal nanoimprint lithography. The template for the nanoimprint process is a replicate from a silica arrayed with nanopillars and fabricated by ICP etching through a SiO_2 colloidal spheres mask. It has been shown that with the internal quasi-periodical scattering gratings the efficiency enhancement can reach 50% for a green light OLED, and with an external antireflection structure, the normal transmittance is increased from 89% to 94% for paraboloid-like pillars. The OLED directly fabricated on the double-sided nanotextured polycarbonate substrate has reached an enhancing factor of ~2.8 for the current efficiency.

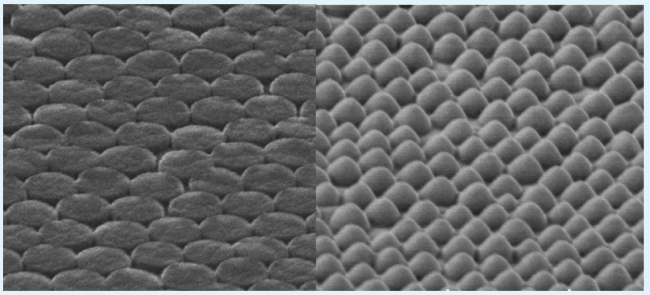

KEYWORDS: *flexible organic light-emitting diode, nanotextured substrate, colloidal lithography, thermal nanoimprint, light extraction*

1. INTRODUCTION

Organic light emitting devices (OLEDs) are attracting more and more attention because of their potential applications in general lighting[1] and flat panel displays.[2] This has been attributed to some desirable features of these devices, such as low power consumption, broad viewing angle, high contrast ratio, high response speed, and flexibility.[3] By using plastic substrates, a flexible OLED (FOLED) (as shown in Figure 1) can be thin and lightweight, therefore promising unique applications in portable or wearable systems, for instance.[4] Although the molecular emitters used in state-of-the-art OLEDs can reach an internal quantum efficiency approaching 100%, the low external quantum efficiencies (EQEs) still restricts the application prospective of OLEDs.[5] The light-emitting mechanism for glass and plastic substrate are basically the same, both suffering from the mismatching in the refractive indices of functional layers of an OLED. Since the organic layers and the typically used ITO anode have a high refractive indices of roughly 2.0 compared to 1.6 for the commonly used plastic substrates, more than 50% of the generated light can be trapped in the device due to a total reflection at the substrate/ITO interface. This loss is called waveguide mode. A similar total reflection also occurs at the substrate/air interface, which can cause an additional loss of about 30% of the generated light) and is called substrate mode. These two modes in combination lead to a final light-extracting efficiency of only 20% in a typical conventional FOLED.

Figure 1. Photography of a finished FOLED device.

Therefore, light extraction in OLEDs has been an active area of research. To out-couple the wave-guided light, OLEDs with surface plasmons,[6] photonic crystal,[7] microcavities,[8] etc. has been proposed. On the other hand, to extract the substrate

Received: March 16, 2014
Accepted: June 16, 2014
Published: June 16, 2014

dx.doi.org/10.1021/am501521p | *ACS Appl. Mater. Interfaces* 2014, 6, 10213−10219

mode light, OLEDs with microlens arrays,[9] antireflection structures,[10] high refractive index substrate[11], etc. have been developed. These works are mostly attempted for out-coupling either mode of light trapped in a device. Bocksrocker[12] has reported a white OLED built on a glass substrate with both internal and external light out-coupling structures. The internal structure was periodical gratings fabricated by laser interference lithography, leading to an average efficiency enhancement of 104%, while the external structure was microlens arrays fabricated by stamping a microlens-arrayed template onto a PMMA/anisole layer on the backside of the OLED, leading to an additional improvement in the efficiency by 94%. Our previous work[13] had adopted a double-sided nanotextured silica as substrate for OLEDs by inductively coupled plasma (ICP) etching following colloidal SiO_2 nanosphere (NS) masking, and the overall current efficiency was enhanced by a factor of 2.8. These works have proved that simultaneously restraining the total reflections through the two modes can create an ultraefficient light extraction for an OLED.

It was also shown that the introduction of nanoscaled structure was also a promising way to suppress the light loss and enhance the out-coupling efficiency for a FOLED. Ho[14] et al. reported a subwavelength antireflection structure consisting of irregularly distributed nanopillars to increase the light extraction efficiency of FOLEDs. The nanopillars were made at polycarbonate substrate/air interface by thermal imprinting from an anodized aluminum oxide (AAO) template. Hsu[15] et al. created a PMMA film with photonic crystal structure and combined it with the FOLED component. However, these methods are faced with problems such as difficulty for large area application, undesirable angle dependent emission spectra, and the need to insert foreign material for the nanopatterning process. At the same time, few efforts have been focused on suppressing the light loss of FOLED from waveguide mode and substrate mode simultaneously.

In this work, a simple method of thermal nanoimprint lithography (NIL)[16] is adopted to fabricate a double-sided nanotextured polycarbonate (PC) flexible substrate. The substrate can out-couple both the light trapped by waveguide mode and substrate mode. The template for NIL is a replicate from a mold which is generated by SiO_2 colloidal lithography[17,18] and ICP etching. For most photonic and grating structures introduced so far for light extraction, the out-coupled light demonstrated a directionality strongly dependent on the specific emission wavelength, polar angle, and azimuthal angle because of their perfectly periodic structure.[19] In our experiment, the nanostructure on the PC/ITO interface is quasi-periodic Bragg-gratings with broad distribution and directional randomness, which will prove to be able to enhance the light-extracting efficiency, yet without introducing spectral changes and directionality. The nanostructure fabricated on the PC/air interface as the antireflection structure (ARS) is composed of subwavelength and paraboloid-like pillars, with which the transmittance reaches 94%, in comparison to 88% for a planar PC substrate. More importantly, it has been found that the current efficiency of the double-sided nanotextured OLED increases by a factor of 2.8, compared with 1.5 by merely introducing a scattering structure at the PC/ITO interface.

2. EXPERIMENTAL DETAILS

The experimental process proposed for the fabrication of FOLEDs includes three major steps, i.e., preparation of templates, thermal NIL, and OLED building.

2.1. Preparation of NIL Template. The preparation of NIL templates is illustrated in Figure 2. To prepare a SiO_2 nanosphere

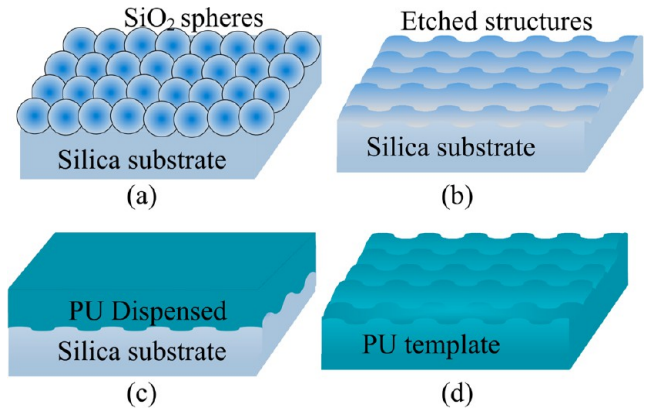

Figure 2. Process for preparation of NIL templates: (a) spin-coating of colloidal SiO_2 spheres on silica, (b) ICP etching of silica, and (c and d) PU template replication from etched silica.

monolayer as etching masks, we synthesize solutions containing colloidal SiO_2 spheres of different diameters dissolved in ethanol. The size distribution of the NPs are 200 ± 20 nm for the ARS at the PC/air interface and 400 ± 50 nm for Bragg-scattering in the PC/ITO interface, respectively, which determines the base diameter of the nanopillars to be etched on the surfaces. First, as shown in Figure 2a, the two-dimensional (2D) colloidal crystals are spin-coated on the substrate as etching masks. The rotating speeds for 200 and 400 nm spheres are 500 and 700 rpm, respectively, and the spin-coating duration for different spheres is identically 30 s. After the spin-coating process, the substrate with a double-sided sphere monolayer is heated at 90 °C for 10 min in the roaster to completely evaporate the solvent. Then the etching process is carried out, as shown in Figure 2b. The spacing, diameter, height, and surface morphology of the nanopillars are controlled by the etching process. Octafluorocyclobutane (C_4F_8) is the reaction gas with silica; O_2 can smooth the etched surface. In our experiments, for the ARS, the etching process is performed with 40 W rf power and additional 400 W ICP power at 5 mTorr in 45 sccm/10 sccm C_4F_8 /O_2 plasma for 4 min to achieve a close-packed and paraboloid-like nanopillar array, since it has been reported that the steadier the transition of the refractive index is, the less the surface reflection is.[18] For scattering structures, as the diameter of spheres is larger, the etching power is raised, with 50 W for rf and 500 W for ICP at the same gases flux for 30 s. The scattering efficiency of grating increases with the depth of grating, but high depth of grating causes a device failure due to high leakage current paths.[20] The depth of gratings is 50 nm in our experiments to ensure no obvious degeneration in electrical properties for FOLED.

Since the etched structures are convex, in order to achieve concave templates used in following thermal NIL, a replication process is executed, as shown in Figure 2c,d, Polyurethane (PU) is selected as replicating resin on account of its abilility to form good nanopatterns and its high mechanical hardness. Before the replication, the etched silica is treated by trichloro(1*H*,1*H*,2*H*,2*H*-perfluorooctyl)silane (FOTS) (Sigma-Aldrich) to lower the surface energy. The PU is composed by isocyanate and polyol at the mass fraction of 100:55. After adequate stirring, the liquid PU is exposed to vacuum for 5 min to get rid of the dissolving air bubbles. Then the PU is dispensed on the etched silica and put in an oven at 70 °C for 1 h. Finally, the PU template is carefully detached from the silica mold.

2.2. Double-Sided Thermal NIL. The thermal NIL process for the PC substrate is shown in Figure 3. The imprinted nanostructures are made on both sides of the PC substrate. Two templates, containing the ARS structure and scattering structure, respectively, are placed to sandwich the substrate, as shown in Figure 3a. The PC substrate is heated on a steel plate with both top and bottom hot plates at a

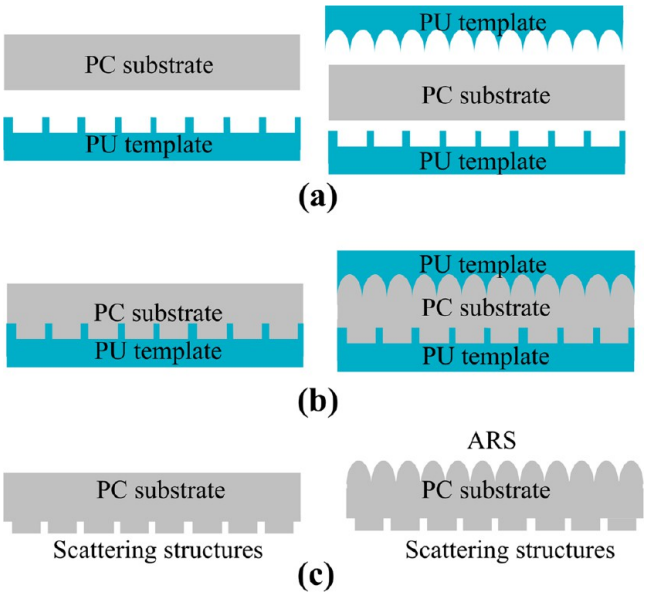

Figure 3. Processes of double-sided thermal NIL: (a) stamp and sample preparation, (b) heating and pressing process, and (c) cooling down and detaching process.

temperature of 150 °C, which is higher than the glass transition temperature of PC. The heated PC film is imprinted by PU templates to form the ARS and scattering structures simultaneously. The pressure is settled at 50 kg/cm^2 so that the nanopores in the template are filled with molten PC, as shown in Figure 3b. After several minutes of imprinting, the whole system is cooled down to room temperature and then the pressure is released. Double-sided structures are formed on the PC substrate after the detaching of the PU templates, as shown in Figure 3c.

2.3. Building of OLED Samples. The green light flexible OLED sample with double-sided structure, the one with an internal Bragg-scattering structure, and a reference device on planar PC substrate are fabricated in our experiment. First, a 200 nm ITO anode is prepared through a low-temperature radio frequency (rf) magnetron sputtering process, without a subsequent high-temperature annealing. The ITO layer is deposited on PC substrate under the radio frequency power of 100 W (corresponding to a chamber temperature of roughly 70 °C), and the base pressure of chamber is lower than 5×10^{-4} Pa. The sheet resistance of the 200 nm ITO anode is around 40 Ω/sq. The other functional layers are prepared by thermal evaporation at a pressure of less than 2×10^{-3} Pa, and 60 nm thick *N*,*N*′-diphenyl-*N*,*N*′-bis(1-naphthylphenyl)-1,1′-biphenyl-4,4′-diamine (NPB) and 60 nm thick tris(8-hydroxyquinoline)aluminum (Alq3) are used as the hole-transporting layer and -emitting layer, respectively. Finally, LiF (1 nm) and Al (150 nm) are used as electron-emitting layer and cathode, respectively. Figure 4a,b illustrates the structures and light emission mode of FOLEDs without and with nanostructures. The luminance–current density–voltage (*L*–*J*–*V*) characteristics are measured. The spectrophotometer and fiber optic spectrometer are utilized to measure the electroluminescent (EL) spectra.

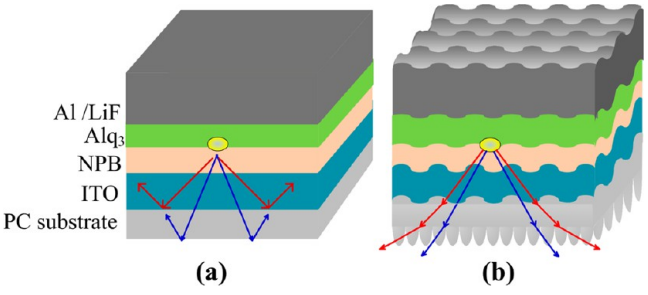

Figure 4. Structures and light propagation illustration of OLED (a) without and (b) with double-sided structures.

2.4. Characterization. The reactive ion etching is carried out in RIE chamber (ICP-180, OXFORD). The thermal NIL process is carried out by a multifunctional chip bonder (Tton-100, AST). The morphological properties of the structures are observed by field-emission scanning electron microscopy (FESEM, SU-8100, Hitachi). The luminance–current density–voltage (*L*–*J*–*V*) characteristics are measured by a source meter (Keithley 2602, Keithley Instruments) and a luminance meter (ST-86LA). The spectrophotometer (PR650, Photo Research) and fiber optic spectrometer are utilized to measure the electroluminescent (EL) spectra.

3. RESULTS AND DISCUSSION

3.1. Nanostructures by NIL. As the sizes of SiO_2 nanospheres in each solutions are not uniform, there are geometrical defects in the array of the assembled sphere monolayer and so are there in the etched silica structure based on it. Figure 5a,b shows the top view SEM images of the monolayer SiO_2 spheres spin-coated on a silica substrate as the mask for the Bragg-scattering structure and ARS, showing that the monolayer is quasi-periodical. Figure 5c,e shows the titled view SEM images of etched silica master and replicated PU template from 400 nm spheres, while Figure 5d,f shows the titled view SEM images of etched silica master and replicated PU template from 200 nm spheres. It is observed that the nanoscale pattern of the master mold was transferred to the PU film with high fidelity. The replicated PU template is then used as an imprint stamp. Figure 5g,h shows the SEM images of the PC substrate thermally imprinted with PU templates, ARS, and scattering structures. According to Figure 5c–h, quasi-periodical nanostructures with different dimensions and topography, identical to etched silica master mold, are formed on the PC substrate.

3.2. The Characterization for OLED Samples Fabricated on Imprinted PC. The OLEDs in our experiments are directly fabricated on the side of PC substrate containing a light-scattering nanostructure. Figure 6 shows the conformal top surface of OLED fabricated on internal structures, demonstrating that the etched structures have been preserved on each layer of the OLED, and the depth of corrugation is shallowed from one layer to another; therefore, effective out-coupling of the waveguide mode is expected.

3.3. *L*–*J*–*V* Performances and Current Efficiency of the FOLED Samples. Figure 7 shows the *L*–*J*–*V* performance of the three devices. Both the device with internal structures and the one with double-sided structures show a higher current density and a higher luminance at a constant voltage, compared with the reference device. The leakage current of devices with internal structures below turn-on voltage is close to that of the reference device, implying a smooth surface of the corrugated structure in the grating device. Due to the corrugated structure, the surface area of the internally textured device is slightly increased by about 15%, which is beneficial for carrier injection and can lower the operating voltage in the grating devices, but the significant enhancement of the current density in the grating device should not be explained by only considering the surface area enhancement. As a matter of fact, it was reported[19,21,22] that an internal textured OLED has a higher current density because of the enhanced electric field due to nonuniformity of the organic layer thicknesses in a corrugated structure. Despite of the increased current density, the higher enhancement of the luminance in the grating device represents

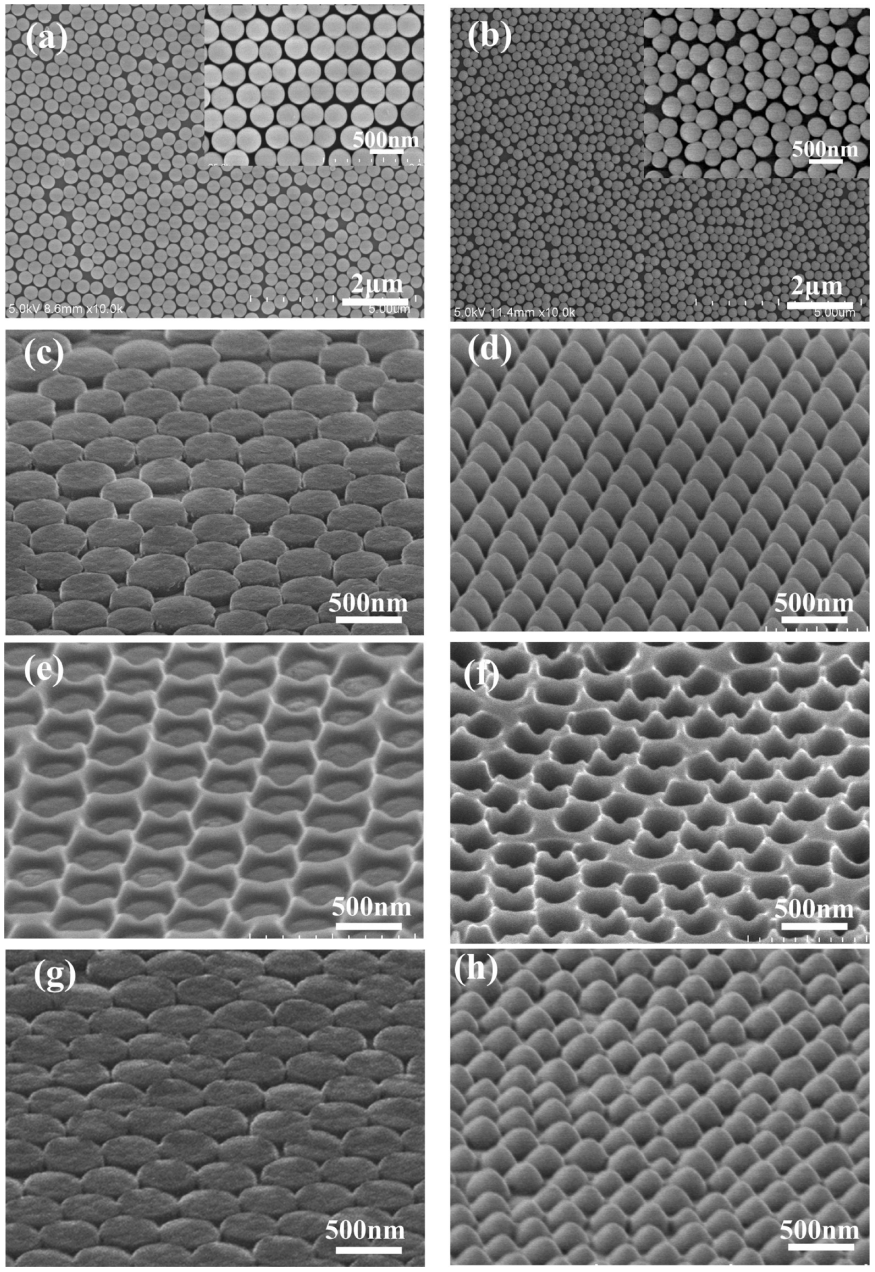

Figure 5. Scanning electron microscopy images of (a and b) spin-coating results of 200 and 400 nm SiO_2 sphere, (c and d) etched structures on silica, (e and f) replicated PU template, and (g and h) thermally imprinted structures on PC substrate.

the extraction of the waveguide modes, as shown in Figure 7a. The scattering efficiency of the grating device increases with the depth of grating, but a high depth of structures can also cause a device failure due to the paths of a high leakage current. In our experiment, the depth of scattering structures is controlled to roughly 50 nm. The devices with internal-scattering structures are lightened for more than 10 h at a constant current of 10 mA and no obvious degeneration in luminance has been observed. However, a surface treatment by coating or sputtering to smooth the patterned substrate would be desirable for preventing the point discharge for organic layers, especially for a device surface patterned to a large depth. Figure 7b shows the current efficiency as a function of luminance for OLEDs fabricated on planar substrate, substrate with internal Bragg-scattering structures, and double-sided nanotextured substrate. The current efficiencies of reference device, internal nanotextured device, and double-sided nanotextured device are 1.9, 2.8, and 5.3, respectively. With internal scattering structures, the current efficiency is enhancing by a factor of 1.5 compared with the reference device, and with an additional ARS, the factor raises up to 2.8.

3.4. Antireflection Property, EL Spectrum, and Angular Dependence Measurements. Figure 8a illustrates the antireflection property of the ARS fabricated at the PC/air interface. The antireflective properties of ARS surfaces are not only broadband but also the best antireflective wave bands depend on the period of the ARS arrays. In our experiment the period of the ARS is around 200 nm and can be used as high performance optics from the ultraviolet to visible light region. The normal transmittance of PC with an ARS is 94.1% at 520 nm compared with 88.8% without the ARS. Furthermore, the transmittance increases during the whole wavelength of visible

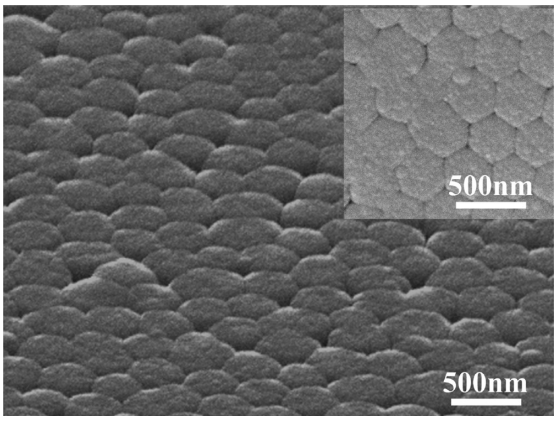

Figure 6. Scanning electron microscopy images of OLED fabricated on an internal scattering structure.

light, and no obvious diversity for different wavelength is observed, indicating that the efficiency enhancement with the ARS is not confined only to certain specific wavelengths. Parts b and c of Figure 8 are the EL spectrum and angular dependence measurements of different OLEDs, respectively. Figure 8b shows the normalized EL spectrum of OLEDs measured from the normal direction at a constant current of 10 mA. The devices containing quasi-periodic scattering structures exhibit enhancement over the entire EL spectrum. The reference device has the peak intensity at a wavelength of 522 nm, and the internally nanotexured and double-sided nanotextured devices achieve the peak intensities at 524 and 526 nm, respectively; no obvious shifts for peak wavelength are observed. The spectrum intensity of double-sided nanotextured OLED is stronger than that ofa single-sided nanotextured one, as the ARS can effectively suppress the total reflection from the substrate mode. The angular dependence of the normalized light intensity for all the devices is shown in Figure 8c. The devices with internal texturing demonstrate patterns quite close to Lambertian emission, with the maximum intensity occurring in the normal direction, which is owing to the quasi-periodic and directional randomness of scattering structures.

Light trapped through the waveguide mode can be extracted by internal nanostructures if the period of the structures satisfies the Bragg-scattering condition. The relationship between the wave vector in free space ($\mathbf{k}_0$) and the wave vector of the in-plane guided mode ($\mathbf{k}_{wg}$) can be written as[19]

$$\mathbf{k}_0 \sin\theta = \mathbf{k}_{wg} \pm n\mathbf{G} \quad (1)$$

where θ is the angle of emitted light, $\mathbf{G}$ is the Bragg vector of the grating, and n is an integer.

The dispersion relation calculated between the wavelength of the emission light that could be recovered and the period of the internal structures in the normal direction is shown in Figure 8d. $\mathbf{G}$ is distributed over all azimuthal directions, because the imprinted structure features have a random orientation. Since the internal-scattering structure in our experiment is quasi-periodical and the range of periodical distribution is between 350 and 450 nm (as illustrated by the dashed lines in the figure), it can be seen that both TE_0 and TM_0 modes of the green light wavelength in the normal direction can be recovered through the structure in the first-order scattering. Additionally, it can be expected that the second-order diffractions of the modes also contribute to the out-coupled emission over all wavelengths. The calculated results are in accordance with the experimental ones shown in Figure 8b. For FOLEDs that emit light of other wavelength, the structure dimensions should be altered according to the corresponding Bragg-scattering condition, which can be easily achieved by synthesizing SiO_2 nanospheres with different diameters and distributions.

4. CONCLUSION

In summary, we have demonstrated that the double-sided thermal NIL on a PC substrate created by using a template fabricated with colloidal lithography is an effective method to increase the out-coupling efficiency of FOLEDs. With this method, an internal quasi-periodic scattering structure and an external antireflection structure can be generated simultaneously on the two sides of the flexible substrate, which is promising for unlocking light losses caused due to the total reflections at the ITO/substrate and at the substrate/air interfaces. Owing to a broadband scattering of the quasi-periodical scattering structure, the green light FOLED with internal nanotexturing exhibits an increase by 50% in the current efficiency without spectral changes and directionality. A FOLED fabricated on a double-sided nanotextured substrate witnesses an enhancing factor of 2.8 for its current efficiency. This method is simple and time-effective as a fabricating process. In addition, the method proposed can be introduced in

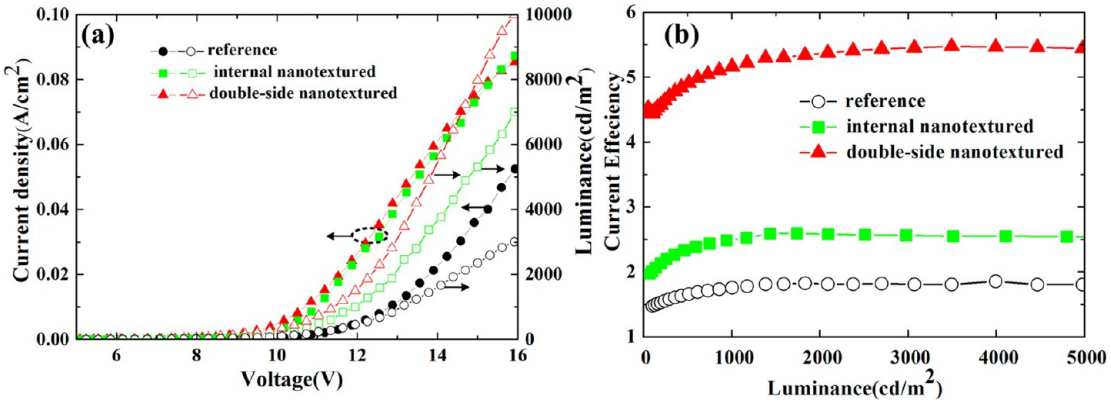

Figure 7. (a) Current density–luminance–voltage characteristics for FOLEDs without structures (black) and with internal structures (green) and double-sided structures (red). (b) Current efficiency as a function of luminance for FOLEDs without structures (black) and with internal structures (green) and double-sided structures (red).

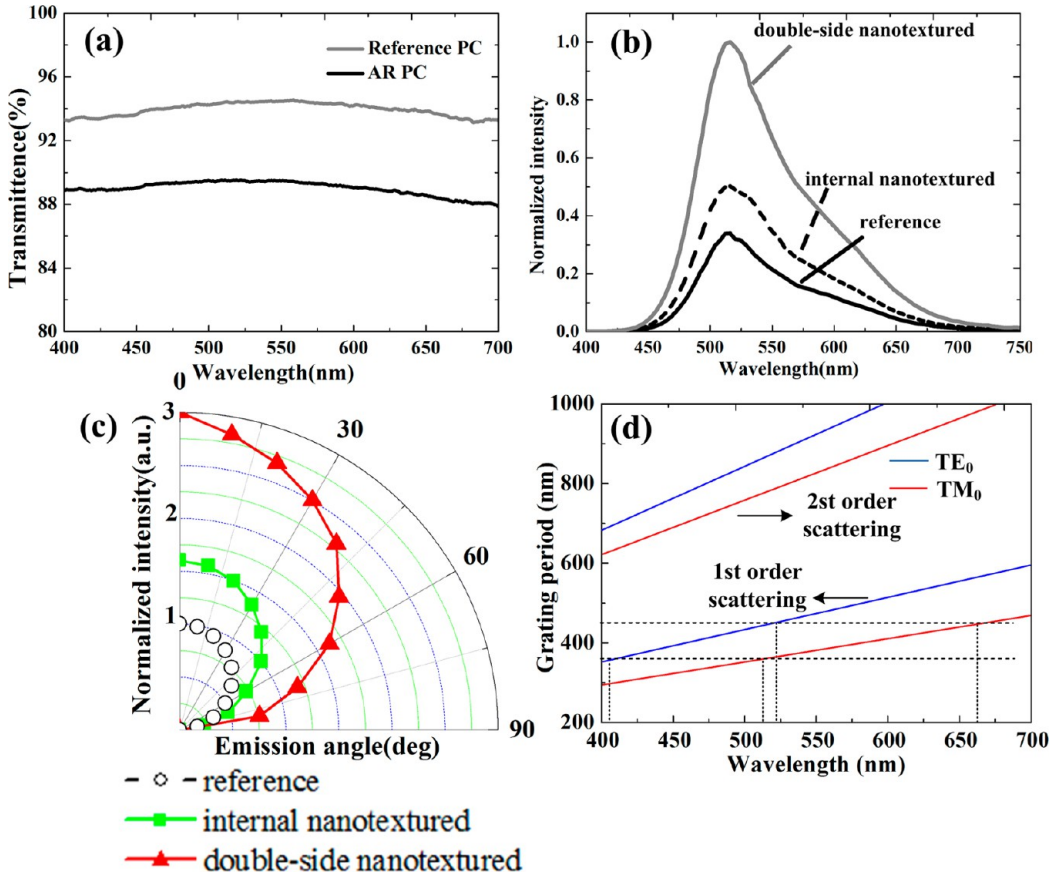

Figure 8. (a)Transmittance of PC substrate with and without an ARS. (b) Spectral intensity and (c) angle independence of light emission from the devices. (d) Relation between the out-coupled emission wavelength in the normal direction and the structure period for the TE_0 (blue) and TM_0 (red) modes.

any FOLEDs without any alteration in the design rule of device structure and materials.

AUTHOR INFORMATION

Corresponding Authors

*L.W. e-mail: wanglime@mail.xjtu.edu.cn.
*Y.D. e-mail: ycding@mail.xjtu.edu.cn.

Notes

The authors declare no competing financial interest.

ACKNOWLEDGMENTS

This work is supported by NSFC Major Research Plan on Nanomanufacturing (Gran No. 91323303 and 51175417), China's National "863" High-Tech Program (Grant No. 2012AA041004), and the Fundamental Research Funds for the Central Universities.

REFERENCES

(1) Sun, Y.; Giebink, N. C.; Kanno, H.; Ma, B.; Thompson, M. E.; Forrest, S. R. Management of Singlet and Triplet Excitons for Efficient White Organic Light-Emitting Devices. *Nature* **2006**, *440*, 908−912.

(2) Sekitani, T.; Nakajima, H.; Maeda, H.; Fukushima, T.; Aida, T.; Hata, K.; Someya, T. Stretchable Active-Matrix Organic Light-Emitting Diode Display Using Printable Elastic Conductors. *Nat. Mater.* **2009**, *8*, 494−499.

(3) McCarthy, M. A.; Liu, B.; Donoghue, E. P.; Kravchenko, I.; Kim, D. Y.; So, F.; Rinzler, A. G. Low-Voltage, Low-Power, Organic Light-Emitting Transistors for Active Matrix Displays. *Science* **2011**, *332*, 570−573.

(4) Forrest, S. R. The Path to Ubiquitous and Low-Cost Organic Electronic Appliances on Plastic. *Nature* **2004**, *428*, 911−918.

(5) Wang, Z. B.; Helander, M. G.; Qiu, J.; Puzzo, D. P. Unlocking the Full Potential of Organic Light-Emitting Diodes on Flexible Plastic. *Nat. Photonics* **2011**, *5*, 753−757.

(6) Wedge, S.; Wasey, J. A. E.; Barnes, W. L. Coupled Surface Plasmon−Polariton Mediated Photoluminescence from a Top-Emitting Organic Light-Emitting Structure. *Appl. Phys. Lett.* **2004**, *85*, 182−184.

(7) Lee, Y. J.; Kim, S. H.; Huh, J.; Kim, G. H. A High-Extraction-Efficiency Nanopatterned Organic Light-Emitting Diode. *Appl. Phys. Lett.* **2003**, *82*, 3779−3781.

(8) Meerheim, R.; Nitsche, R.; Leo, K. High-Efficiency Monochrome Organic Light Emitting Diodes Employing Enhanced Microcavities. *Appl. Phys. Lett.* **2008**, *93*, 043310.

(9) M?ller, S.; Forrest, S. R. Improved Light Out-Coupling in Organic Light Emitting Diodes Employing Ordered Microlens Arrays. *J. Appl. Phys.* **2002**, *91*, 3324−3327.

(10) Li, Y.; Li, F.; Zhang, J.; Wang, C. Improved Light Extraction Efficiency of White Organic Light-Emitting Devices by Biomimetic Antireflective Surfaces. *Appl. Phys. Lett.* **2010**, *96*, 153305.

(11) Nakamura, T.; Tsutsumi, N.; Juni, N. Thin-Film Waveguiding Mode Light Extraction in Organic Electroluminescent Device Using High Refractive Index Substrate. *J. Appl. Phys.* **2005**, *97*, 054505.

(12) Bocksrocker, T.; Preinfalk, J. B.; Asche-Tauscher, J.; Pargner, A. White Organic Light Emitting Diodes with Enhanced Internal and External Outcoupling for Ultra-Efficient Light Extraction and Lambertian Emission. *Opt. Express* **2012**, *20*, 932−940.

(13) Luo, Y.; Wang, L.; Ding, Y.; Li, L. High Light-Extracting Efficiency for OLED Directly Fabricated on Double-Side Nano-textured Silica Substrate. *Opt. Lett.* **2013**, *38*, 2394−2396.

(14) Ho, Y. H.; Liu, C. C.; Liu, S. W.; Liang, H. Efficiency Enhancement of Flexible Organic Light-Emitting Devices by Using Antireflection Nanopillars. *Opt. Express* **2011**, *19*, 295−302.
(15) Hsu, Q. C.; Hsiao, J. J.; Ho, T. L. Fabrication of Photonic Crystal Structures on Flexible Organic Light-Emitting Diodes Using Nanoimprint. *Microelectron. Eng.* **2012**, *91*, 178−184.
(16) Chou, S. Y.; Krauss, P. R.; Renstrom, P. J. Renstrom Imprint of Sub 25 nm Vias and Trenches in Polymers. *Appl. Phys. Lett.* **1995**, *67*, 3114−3116.
(17) Zhang, J.; Li, Y.; Zhang, X.; Yang, B. Colloidal Self-Assembly Meets Nanofabrication: From Two-Dimensional Colloidal Crystals to Nanostructure Arrays. *Adv. Mater.* **2010**, *22*, 4249−4269.
(18) Li, Y.; Zhang, J.; Yang, B. Antireflective Surfaces Based on Biomimetic Nanopillared Arrays. *Nano Today* **2010**, *5*, 117−127.
(19) Koo, W. H.; Jeong, S. M.; Araoka, F.; Ishikawa, K. Light Extraction from Organic Light-Emitting Diodes Enhanced by Spontaneously Formed Buckles. *Nat. Photonics* **2010**, *4*, 222−226.
(20) Fujita, M.; Ishihara, K.; Ueno, T.; Asano, T. Optical and Electrical Characteristics of Organic Light-Emitting Diodes with Two-Dimensional Photonic Crystals in Organic/electrode Layers. *Jpn. J. Appl. Phys.* **2005**, *44*, 3669−3677.
(21) Fujita, M.; Ueno, T.; Ishihara, K.; Asano, T. Reduction of Operating Voltage in Organic Light-Emitting Diode by Corrugated Photonic Crystal Structure. *Appl. Phys. Lett.* **2004**, *85*, 5769−5771.
(22) Jeong, S. M.; Araoka, F.; Machida, Y.; Ishikawa, K. Enhancement of Normally Directed Light Outcoupling from Organic Light-Emitting Diodes Using Nanoimprinted Low-Refractive-Index Layer. *Appl. Phys. Lett.* **2008**, *92*, 083307.